Environmental Science & Technology

pubs.acs.org/est

Article

Contributions of Coagulation, Deposition, and Ventilation to the Removal of Airborne Nanoparticles in Indoor Environments

Su-Gwang Jeong, Lance Wallace, and Donghyun Rim*

Cite This: https://doi.org/10.1021/acs.est.0c08739

Read Online

ACCESS | Metrics & More | Article Recommendations | Supporting Information

ABSTRACT: Airborne nanoparticles are frequently released in occupied spaces due to episodic indoor source activities. Once generated, nanoparticles undergo aerosol transformation processes such as coagulation and deposition. These aerosol processes lead to changes in particle concentration and size distribution over time and accordingly affect human exposure to nanoparticles. The present study establishes a framework for an indoor particle dynamic model that can predict time- and size-dependent particle concentrations after episodic indoor emission events. The model was evaluated with six experimental data sets obtained from previous measurement studies in the literature. The indoor particle dynamic model quantified the relative contributions of three particle loss mechanisms (i.e., coagulation, deposition, and ventilation) to the total reduction in number concentration. The results show that particle coagulation and indoor surface deposition are two dominant processes responsible for temporal changes in particle size and concentration following indoor emission events. The first-order equivalent coagulation loss rate notably varies with indoor emission source and accounts for up to 59% of the total particle loss for burning a candle, 42% for broiling a fish, and 10% for burning incense. The results reveal that while the coagulation loss rate changes markedly with the particle concentration and source type, the deposition loss rate is more dependent on particle size. Compared to coagulation and deposition, the effect of ventilation is marginal for most of the nanoparticle emission events indoors; however, ventilation loss becomes pronounced with the decrease of particle concentration below 5×10^4 cm^{-3}, especially for particles larger than 100 nm in aerodynamic diameter.

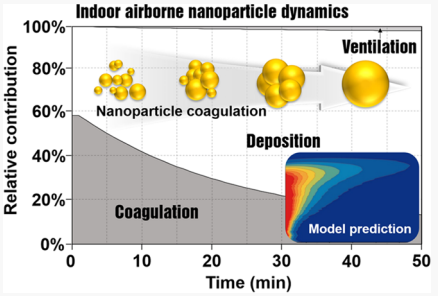

KEYWORDS: *indoor air, aerosol dynamic model, ultrafine particles, particle size distribution, indoor activities*

INTRODUCTION

Inhalation exposure to airborne particulate matter (PM) is one of the major environmental risk factors that increase the burden of diseases worldwide.[1] Studies have shown that human exposure to PM is associated with adverse health effects, such as respiratory, neurological, and cardiovascular diseases.[2−7] Although PM exposure is attributed to both outdoor and indoor emission sources,[8,9] a large portion of the population exposure to PM occurs indoors, given that people spend a majority of their time in enclosed spaces and even longer under extreme events such as wildfires or infectious disease pandemics.[10−12] Indoor PM emission events are typically episodic and can lead to high concentrations of airborne nanoparticles.[13,14] Several studies revealed that oxidative stress caused by nanoparticles is more toxic than that due to larger particles of the equivalent mass because of the large surface area available for biological and chemical interactions with human cells.[15−17] Previous studies measured the size-dependent particle concentrations associated with indoor activities and quantified daily PM exposure.[18−22] Their results reveal that human activities such as cooking, burning candles, smoking, solid fuel combustion, walking, or use of electric appliances contribute to increases in indoor particle concentrations.[23−29]

Once particles are emitted from an indoor source, the particles undergo aerosol transformation processes such as coagulation, deposition, and ventilation.[30−33] Such processes play major roles in changes of particle size and concentrations with time. In particular, when particle number concentrations are high due to source emissions in a relatively small indoor occupied space, coagulation loss can be significant for nanoparticles smaller than 50 nm.[30,33] During the coagulation process, particles collide and stick with one another, creating larger particles. Over this process, the total particle number concentration decreases with time while the particle size distribution shifts toward larger particles.[34] Several studies reported dynamic changes in particle number concentrations and source emission rates resulting from different indoor sources.[14,23,26,33−36] Lai et al.[37] performed experiments in a small-scale chamber and monitored particles in a size range of 14−250 nm. Based on the measurement, they developed a

Received: December 26, 2020
Revised: May 27, 2021
Accepted: May 28, 2021

particle dynamic model that estimated five different coagulation mechanisms including van der Waals, viscous forces, and fractal effects. The modeled particle number concentrations matched well with the measurement data, and the results suggested that coagulation and convective transport are the main processes responsible for changes in indoor particle concentration during high-concentration periods. Géhin et al.[38] measured the particle size distributions associated with 18 different indoor activities (burning candle or incense, cooking, spray use, computer printing, and household cleaning). This study demonstrates that a number of ultrafine particles (<100 nm in size) are emitted during indoor human activities and the highest concentrations were found while cooking meat or fish on a stove and during pyrolysis oven cleaning. Stabile et al.[39] measured newly generated ultrafine particles when using floor cleaning products. Based on multiple chamber tests with 20 different products (mostly containing VOCs and surface agents), 10 cleaning products were identified as nanoparticle-generating products for the nucleation range (about 10 nm). Wang et al.[40] investigated the size-resolved deposition rate and Brownian coagulation coefficient for the aerosolized SiO_2 nanoparticles with concentrations of about 6.0×10^4 cm^{-3} at relative humidity (RH) values of 9−64% in a laboratory chamber. Except for the extremely dry condition (9% RH), 40−50% of the total particle loss at the beginning of decay was associated with coagulation. However, few studies have examined detailed effects of indoor particle loss mechanisms on size and concentration dynamics for common emission sources in full-scale, realistic buildings.[33]

Given this background, the objectives of this study are to (1) establish an indoor aerosol dynamic model that predicts time- and size-dependent concentrations after episodic source releases and (2) quantify relative contributions of coagulation, deposition, and ventilation to indoor particle losses after nanoparticle emission events. The aerosol dynamic model developed herein is evaluated with the actual measurement data published in the literature and can help predict indoor particle dynamics and human exposure associated with episodic indoor nanoparticle emissions.

METHODS

The indoor aerosol dynamic model was established and validated using experimental data sets published in the literature based on field measurements in full-scale residential buildings. These studies monitored time- and size-resolved particle concentrations associated with six typical indoor emission sources: a candle, a gas stove, a clothes dryer, a toast, a broiled fish, and an incense.[26,33,34,36,41] The measurement data were collected from three different homes located in Santa Rosa, CA (candle), Gaithersburg, MD (gas stove), and Reston, VA (remaining four sources). For the measurements in the whole house, we used the experimental data collected with the central mixing fan operating in the entire house. Figure 1 summarizes the particle number concentrations due to the six indoor sources at the start of decay observed in those studies. Each data set shows a distinct particle size distribution with regards to the geometric mean, geometric standard deviation (GSD), and total number concentration. We focused on the particle decay period to examine how the aerosol size/concentration dynamics vary with indoor source due to different indoor particle loss mechanisms. The initial decay data reflect the effects of source emission on the particle size distribution and number concentration. Detailed information

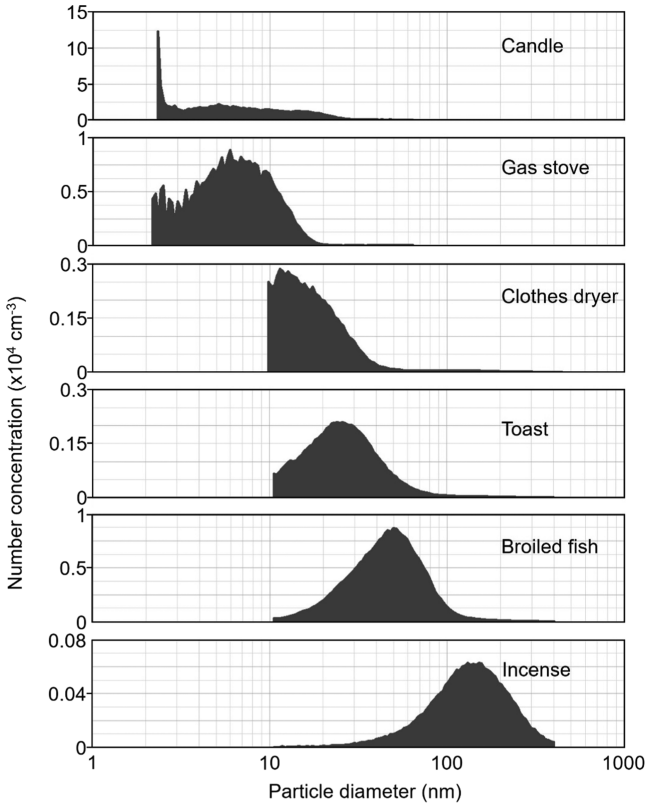

Figure 1. Size-resolved number concentrations due to the six indoor sources at the start of the decay.[33,34,36]

about all six tests including house volume, air change rate, and measured particle size range is provided in the Supporting Information (see Tables S1 and S2).

Characterization of Size-Resolved Particle Concentrations Using a Log-Normal Distribution. We hypothesized that a measured particle size distribution can be modeled as a log-normal distribution with a specific geometric mean diameter (GMD) and a geometric standard deviation (GSD). The values of GMD and GSD were calculated based on the following three equations.[42]

$$\ln \bar{G}_D = \frac{1}{N_T} \sum_{i=1}^{N_{Bin}} (n_i \ln d_i) \quad (1)$$

$$N_T = \sum_{i=1}^{N_{Bin}} n_i \quad (2)$$

$$\ln \sigma_G = \sqrt{\frac{1}{N_T} \sum_{i=1}^{N_{Bin}} \left(n_i \ln^2 \frac{d_i}{\bar{G}_D} \right)} \quad (3)$$

where $\bar{G}_D$ is the GMD, N_T is the total number concentration (cm^{-3}) summed over all particle size bins, and n_i is the number concentration of particles in the size bin i. N_{Bin} is the total number of size bins, d_i is the particle diameter in the size bin i, and σ_G is the GSD.

Once the total number concentration, GMD, and GSD were determined, the log-normal distribution was modeled as follows.[42]

https://doi.org/10.1021/acs.est.0c08739
Environ. Sci. Technol. XXXX, XXX, XXX−XXX

$$n_j = \frac{N_T \Delta d_j}{d_j \sqrt{2\pi}\ \ln\ \sigma_G} \exp\left[-\frac{\ln^2(d_j/\overline{G}_D)}{2\ln^2\sigma_G}\right] \quad (4)$$

where n_j is the number concentration in the size bin j and d_j is the particle diameter of the size bin j.

Indoor Particle Dynamic Model. Based on the log-normal particle distribution, the dynamic behavior of the size-resolved particle number concentration was modeled using a material balance model that calculated the particle gain due to coagulation and particle losses from coagulation, deposition, and ventilation, as shown in eq 5.

$$\frac{\partial n(v,t)}{\partial t} = \frac{1}{2}\int_{v_0}^{v-v_0} \beta(v-\overline{v},\overline{v})n(v-\overline{v},t)n(\overline{v},t)\mathrm{d}\overline{v} - n(v,t)\int_{v_0}^{\infty}\beta(\overline{v},v)n(\overline{v},t)\mathrm{d}\overline{v} - (k+a)n(v,t) \quad (5)$$

where $n(v,t)$ $[m^{-3}]$ is the particle number concentration for particle volumes $[m^3]$ between v and $v + dv$ at time t $[s]$; $v - \overline{v}$ and $\overline{v}$ are the volumes of two colliding particles; v is the volume of the newly coagulated particle; β is the coagulation kernel (collision rate coefficient); k is the particle deposition rate $[h^{-1}]$; and a is the air exchange rate $[h^{-1}]$. The first two integrals on the right-hand side represent the particle gain and loss due to coagulation, respectively. The third term on the right side represents the particle loss due to deposition and ventilation.

Using eq 5, time-varying particle size distributions in the range of 2−400 nm were calculated with each time step of 1 s. The time step of 1 s for the numerical solution was based on the coagulation time scale for 2−3 nm particles.[33,42] For modeling the coagulation process, the semi-implicit method that used volume fraction factors to preserve the total volume concentration at each time step was employed.[42] The coagulation kernel (β) represents the second-order rate constant that reflects a collision rate between two particle clusters that is affected by several factors including Brownian motion, van der Waals force, viscous force, fractal geometry, convective Brownian enhancement, gravitational sedimentation, and turbulent motions.[30−32] A previous study[43] presented a methodology to predict and estimate the best-fit input parameters for the current indoor aerosol model considering Brownian diffusion as the coagulation kernel. A few other studies examined the effective coagulation coefficient from the steady-state model using the Fuchs coagulation kernel and considering the effect of fractal agglomerate on particle number, surface area, and mass concentrations.[44,45]

In the present study, Brownian motion with the Fuchs correction as well as van der Waals and viscous forces was taken into account to estimate β (see Figure S2). Detailed information on modeling coagulation is provided in the Supporting Information (see Modeling of Coagulation in the SI). The Hamaker constant, which represents the binding potential due to van der Waals force, was set to 20 k_BT (where k_B is the Boltzmann constant and T is the absolute temperature), which was shown to work reasonably well for indoor organic particles.[14,33,36] As coagulation is a second-order process, the coagulation loss rate increases proportionally to the square of the particle concentration. However, to evaluate how the coagulation loss rate changes with time compared to deposition and ventilation loss rates, the first-order equivalent loss rate due to coagulation was estimated for a specific time interval as follows

$$k_{c,i}(t) = -\ln\left(\frac{\Delta N_i(t)}{N_{0,i}}\right)/t = -\ln\left(\frac{\text{initial number of particles} - \text{number of coagulation loss}}{\text{initial number of particles}}\right)/t \quad (6)$$

where $k_{c,i}$ (t) is the first-order equivalent coagulation loss over a time interval t for the particle size bin i, $\Delta N_i(t)$ is the number concentration reduced by the number of coagulation loss over the time interval t, and $N_{0,i}$ is the initial number concentration for the particle size bin i.

The particle dynamic model is based on the time-varying particle size distribution and the air change rate; however, note that the model does not distinguish indoor environmental settings. The effects of specific environmental conditions (i.e., surface-to-volume ratios, roughness of the surfaces, airflow conditions) are reflected in the particle concentration and air change rate, based on which the model predicts the concentration profiles and relative importance of coagulation, deposition, and ventilation on the particle dynamics.

Estimation of Deposition Rates. Along with time-dependent coagulation losses, particle deposition rates were estimated for the six indoor sources using an iteration method.[36] Deposition rates were typical of building conditions due to indoor airflow, surface areas, filtration, and air conditioning mode; the size-resolved deposition rates were estimated for each test. A previous study[36] validated this iteration method based on the field measurement data. A detailed description of the iteration method is provided in the paper; however, briefly describing the iteration process, we initially assumed a set of deposition rates for different particle sizes and particle number concentrations were then calculated for each time step of the decay period. The initial deposition rates were based on the indoor particle deposition theory;[46−48] however, it turned out that the initial values made minimal differences to the converged solution. At each time step, the errors for the deposition rate estimates were calculated as the square sum of differences between the simulated and measured number concentrations. Note that for each iteration, we estimated the deposition rate as the difference between the total particle loss and the sum of coagulation and ventilation losses. Size-specific deposition rates were updated iteratively until the sum of errors for the whole decay period was obtained with the specific convergence criterion ($\sum|k_e^{n+1} - k_e^n| \le 10^{-2}$), where k_e indicates the estimated deposition rates.

RESULTS AND DISCUSSION

Six Episodic Events Representing Different Particle Size Distributions. Table 1 summarizes the percentages of particles in seven particle size bins ranging from 2 to 400 nm for six indoor emission sources observed in the previous experimental studies.[33,34,36] For all indoor sources, the total particle number concentrations at the beginning of decay varied from 21 000 to 1100 000 cm^{-3}. For the candle burning, high concentrations (>510 000 cm^{-3}) were observed with 47% of the total particles in the 2−5 nm size range. The gas stove also showed relatively high total number concentrations (>140 000 cm^{-3}), with about a half of the total within the size range of 5−10 nm. The clothes dryer and toast produced smaller numbers of particles (73 000 and 67 000 cm^{-3}), but

https://doi.org/10.1021/acs.est.0c08739
Environ. Sci. Technol. XXXX, XXX, XXX−XXX

Table 1. Percentage of Particles in Different Size Ranges for the Six Indoor Sources

	percentage particle number concentration (%)						
activity	2–5 nm	5–10 nm	10–18 nm	18–40 nm	40–100 nm	100–200 nm	200–400 nm
candle[36]	46.8	28.8	17.5	6.5	0.4	0	0
gas stove[33]	37.0	47.1	15.3	0.5	0.2	0	0
clothes dryer[34]	0	3.4	56.4	36.7	2.2	1.0	0.3
toast[34]	0	0	23.2	62.0	13.9	0.7	0.2
broiled fish[34]	0	0	3.9	35.1	57.7	3.0	0.3
incense[34]	0	0	0.3	2.6	25.3	51.5	20.3

more larger particles with about 55% of the total in a size range of 10–40 nm. Note that broiled fish produced a majority of particles in the 40–100 nm range, with a relatively high total particle number concentration (258 000 cm^{-3}). Among the six sources, the incense produced the biggest particles with more than 70% of particles in the size range of 100–400 nm, while the particle number concentration was the lowest. Given that each emission source yields a distinct particle size distribution, the dominant particle loss mechanisms are expected to be different for the six different emission sources.

Figure 2a–f compares log-normal particle size distributions for the six indoor sources that are fitted based on the measurement data. The log-normal distributions were calculated for the particle size range of 2–400 nm. The figures show that each indoor source event can be fitted to a log-normal distribution, with the root mean square error (RMSE) values of 287 for candle, 62.2 for gas stove, 6.95 for clothes dryer, 5.35 for toast, 33.8 for broiled fish, and 1.59 for incense. Although particle size distribution widely varies with source type, unimodal log-normal distribution function with a single set of GMD and GSD[36,37] fits well for most of the indoor sources except for the candle. As for the candle, the particle size distribution is better characterized by a bimodal log-normal distribution, with the first concentration peak in the range of 2–3 nm and the second peak in 5–6 nm. The R^2 values between log-normal size distribution and measurement data for six sources are 94.1% for candle, 91.1% for gas stove, 98.9% for clothes dryer, 98.6% for toast, 95.3% for broiled fish, and 99.2% for incense. Although these fittings provide reasonable accuracy for our model, the model accuracy may increase further with refining the size distribution to bimodal or trimodal distribution.

Based on these log-normal distributions as initial conditions, the following section presents results of the indoor particle dynamic model as well as the roles of aerosol processes (ventilation, deposition, and coagulation) in the dynamics of particle size and concentration.

First-Order Equivalent Coagulation Loss Rates. Figure 3a,b presents the first-order equivalent coagulation loss rates

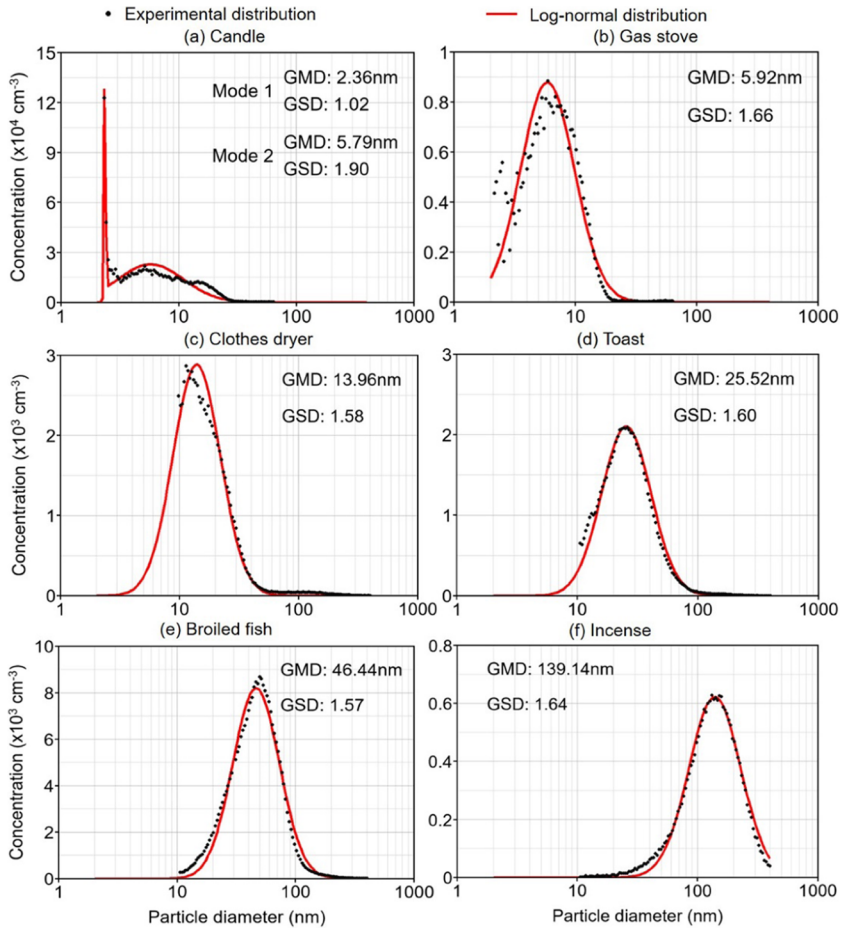

Figure 2. Comparison of size-resolved particle number concentrations between experiment and log-normal distribution fitting for six indoor nanoparticle emission sources: (a) candle,[36] (b) gas stove,[33] (c) clothes dryer,[34] (d) toast,[34] (e) broiled fish,[34] and (f) incense.[34]

https://doi.org/10.1021/acs.est.0c08739
Environ. Sci. Technol. XXXX, XXX, XXX–XXX

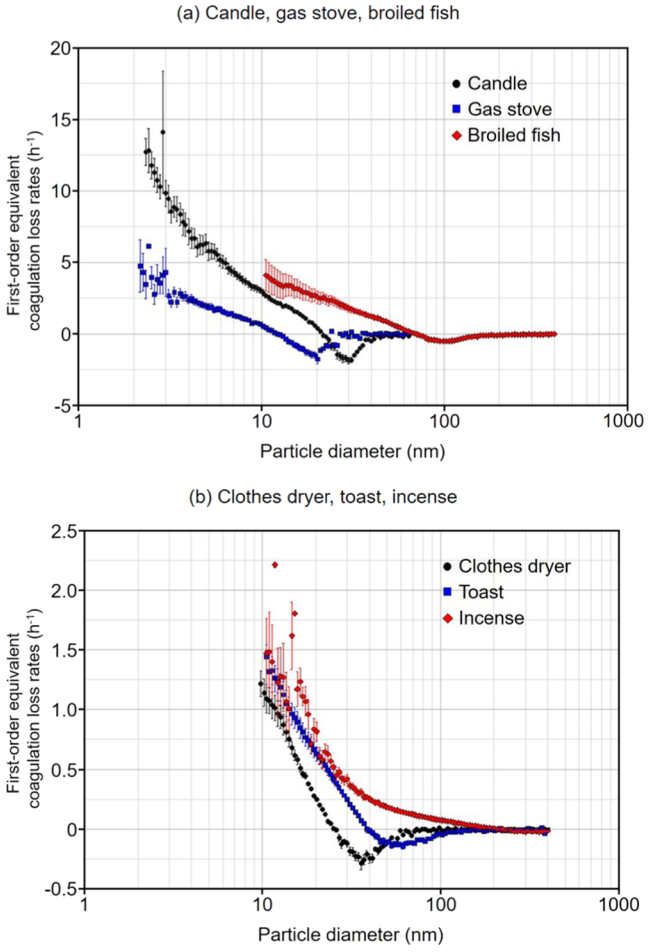

Figure 3. Size-resolved first-order equivalent coagulation loss rates for (a) candle,[36] gas stove,[33] and broiled fish[34] and (b) clothes dryer,[34] toast, and[34] incense.[34] Note that the error bars represent the standard error and the *Y*-axis scale is 10 times larger for (a) than that for (b).

for the initial 25 min of the decay period and how coagulation loss varies with source emission type and particle size. According to the figures, although particle size distributions are different for the six sources, in general, the smaller the particle, the higher the coagulation loss rate. This result suggests that coagulation has a more significant impact on the dynamics of smaller particles, mainly due to the high particle collision rate.[49,50] In the case of the candle, the first-order equivalent coagulation loss rate is as high as 13 h^{-1} for the size range of <10 nm, which is much higher than other indoor sources. Note that coagulation is a second-order process involving particle number concentrations; if the number concentration is doubled, the coagulation effect would be 4 times higher.[13] Broiled fish yields coagulation loss rates of 2.5−5 h^{-1} in the particle size range of 10−20 nm. It is interesting to see that these rates are higher than those of clothes dryer and toast (<1.5 h^{-1}) (see Figure 3b). Although broiled fish produces more larger particles than clothes dryer and toast, they yield larger coagulation losses because of higher particle number concentrations.

It should be noted that in Figure 3, negative loss rates reflect particle gain because of coagulation. Candle and gas stoves showed clear particle gains between 20−40 nm and 10−40 nm, respectively. In the case of the candle, the initial particle number concentration was high for the size range of <20 nm and coagulation led to particle gain in the size range of 20−40 nm (see Figure S1). The gas stove produced most particles <10 nm, which resulted in coagulation gains for particles larger than 10 nm. These results were attributed to the differences in size distribution and number concentration between the two sources. Comparatively much smaller particle gains occurred for broiled fish than those for candle and gas stove. For the incense, the particle gain due to coagulation was negligible (Figure 3b), which was mainly attributed to a relatively low total particle number concentration and a high GMD of the particle size distribution. As a result, the coagulation loss rate was higher for the sources (candle, gas stove, broiled fish) with a large number of particles during the initial 25 min after the beginning of decay. In addition, we observed that as the number concentration decreased due to coagulation, the coagulation gain tended to gradually decrease with time. These results demonstrate that the coagulation loss rate is meaningfully influenced by both particle number concentration and size distribution. Figure S3 provides detailed time-varying coagulation loss rates for the six sources.

Deposition Rates. Figure 4 presents size-resolved particle deposition rates for each indoor source obtained from the iteration method.[36] Note that deposition rates were estimated only for particle size bins that had particle number concentrations higher than 100 cm^{-3} at the beginning of decay, considering relatively high estimation uncertainties with lower concentrations. Previous studies reported that deposition rates followed a log-linear curve with high R^2 values up to 99% for the nanoparticle size range <100 nm.[33,36] In our analysis, for the data from candle, gas stove, toast, broiled fish, and incense, the R^2 values of the log-linear curve ranged from 88.3 to 96.6%, while it was much lower for incense (60.7%). It is important to mention that the data from the clothes dryer did not show a log-linear curve, implying other potential aerosol transformation processes (e.g., evaporation) occurring with this emission source. In the clothes dryer case, the deposition rate tended to increase with particle size in the range of 10−20 nm, which was opposite to the theoretical prediction of the size-dependent particle deposition.[46,47,51] We speculate that particles released from clothes dryer contain moisture and they evaporate after being released in the indoor air, which leads to a notable decrease in particle number and is reflected as the deposition rate increase in the size range of 10−20 nm. The

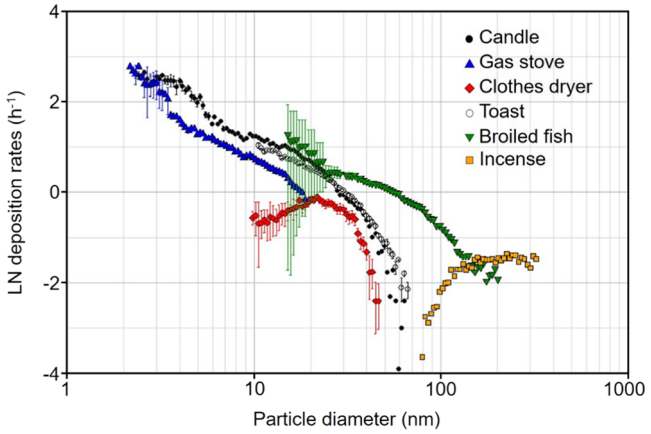

Figure 4. Size-resolved deposition rates for the six indoor sources. Note that the *y*-axis is in the natural logarithmic (LN) scale and the error bars represent standard errors.

https://doi.org/10.1021/acs.est.0c08739
Environ. Sci. Technol. XXXX, XXX, XXX−XXX

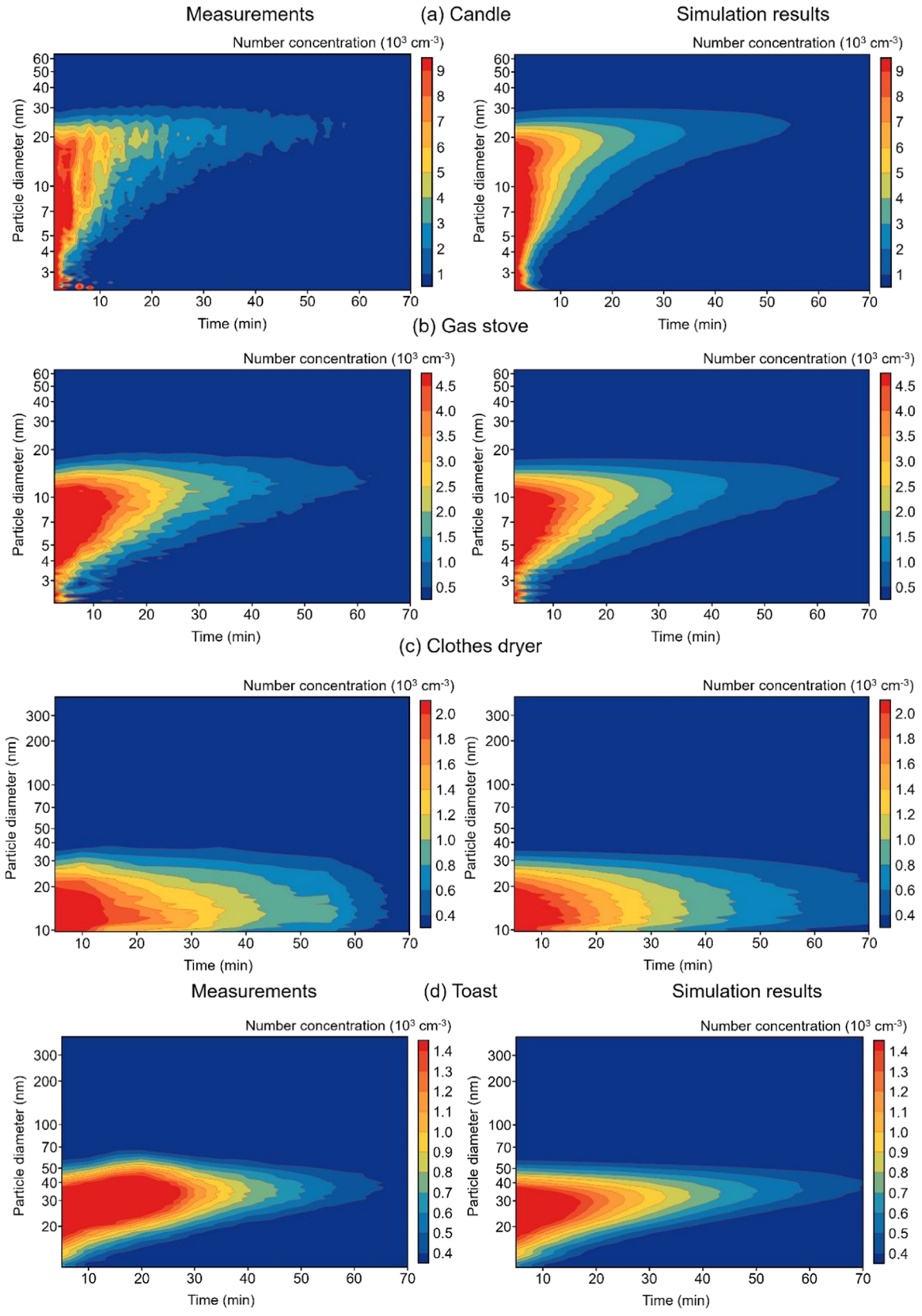

Figure 5. continued

https://doi.org/10.1021/acs.est.0c08739
Environ. Sci. Technol. XXXX, XXX, XXX−XXX

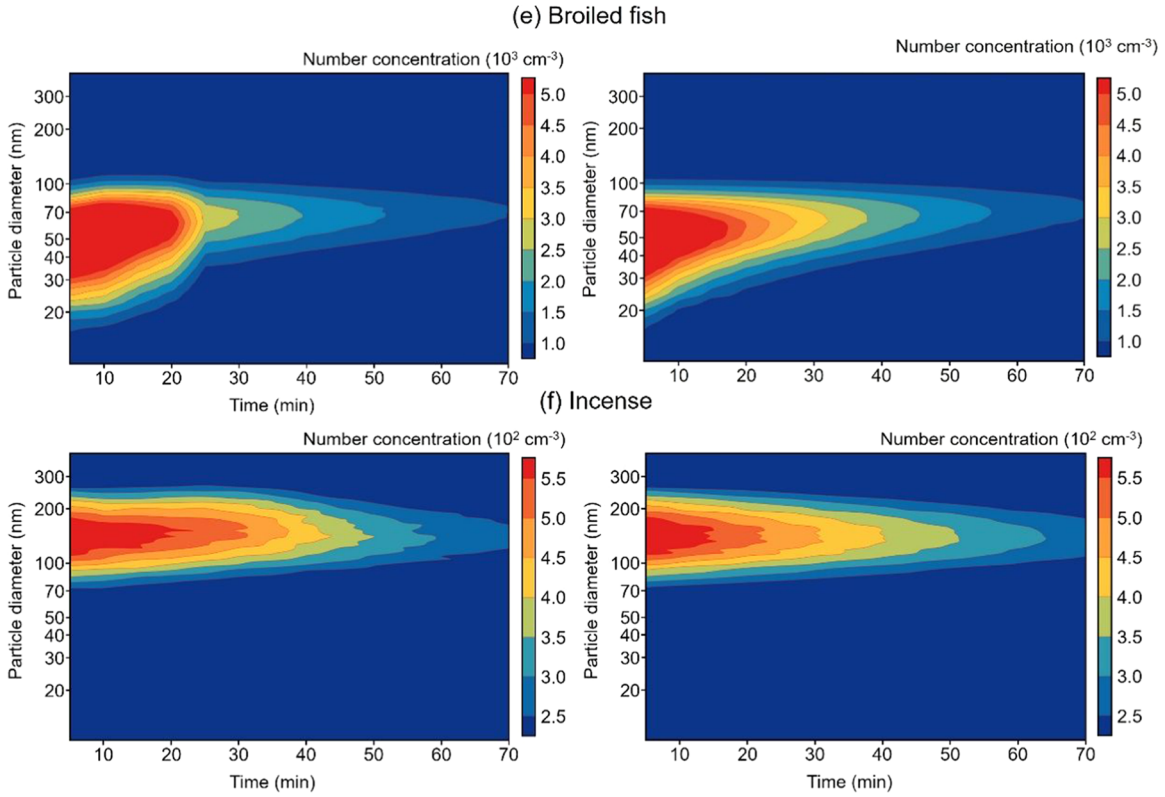

Figure 5. Measurement vs model: time-dependent particle size distributions: (a) candle,[36] (b) gas stove,[33] (c) clothes dryer,[34] (d) toast,[34] (e) broiled fish,[34] and (f) incense.[34]

deposition rate estimates decreased as particle size increased in the range of 2−70 nm except for the case of clothes dryer. This result supports previous findings that the particle deposition to indoor sources is enhanced for smaller particles (<50 nm) due to Brownian and turbulent diffusion.[46−48,50,52] The detailed size-dependent deposition rates for the six indoor sources are presented in Figure S4.

Particle Size Distributions: Measurements vs Model Predictions. Figure 5a−f compares the modeled and observed time-varying particle size distributions for all six indoor sources. Note that the initial particle size distribution was the same for the model and the measurement data. The subsequent modeled time series were based on the coagulation and deposition rates presented above. The figures show similar trends in the temporal variation of particle size distributions between measurements and model results, although some discrepancies appear in the early decay period, perhaps due to incomplete air mixing in the measurements in full-scale buildings. Figure 4a shows that the majority of particles emitted from the candle are smaller than 20 nm and the particle size distribution shifts toward larger sizes with time. The model captures reasonably well that particle number concentrations quickly decrease in the small particle size range with the increase of geometric mean diameter over time. The simulation results of both candle burning and gas stove reveal strong coagulation effects attributed to high collision rate and high concentrations of nanoparticles smaller than 10 nm (Figure 5a,b). Figure 5c shows the results of clothes dryer, in which high particle number concentrations were maintained for a relatively long time (>20 min) likely due to evaporation of larger particles. In such a case, the model could underestimate the coagulation losses. Future studies can investigate the detailed effects of evaporation for unvented clothes dryers in addition to coagulation and deposition. For the experiments with indoor cooking activities (toast and broiled fish), particle emission from the source occurred in the kitchen, while the measurement was performed in the basement with the central mixing fan operating in the whole house. Due to this condition, there were time delays (8−10 min) for particles generated from the source to spread to the basement. Excluding such delays and activities that are not modeled (e.g., opening the oven door around 25 min for the broiled fish), the simulation results reproduce the dynamic evolution of particle size distributions with reasonable accuracy. However, it should be noted that this study has a limitation assuming the spatial homogeneity of particle number concentration between the emission source and the measurement location. Regarding incense burning, the model prediction is in good agreement with the experimental data in the particle size range of 80−300 nm. The results suggest that the indoor particle dynamic model can simulate the temporal changes in the particle size and concentration associated with individual loss mechanisms. The model can provide meaningful insights into the dominant aerosol processes considering the emission source type and building conditions. The following section discusses the detailed aerosol transformation processes for different indoor emission source types.

Relative Contributions of Coagulation, Deposition, and Air Change to Particle Loss. Figure 6a−f shows the relative contribution to particle number concentration loss in time during the decay for the six indoor sources. The figures reveal information of major particle loss mechanisms at a specific time of the decay, depending on the source type and

https://doi.org/10.1021/acs.est.0c08739
Environ. Sci. Technol. XXXX, XXX, XXX−XXX

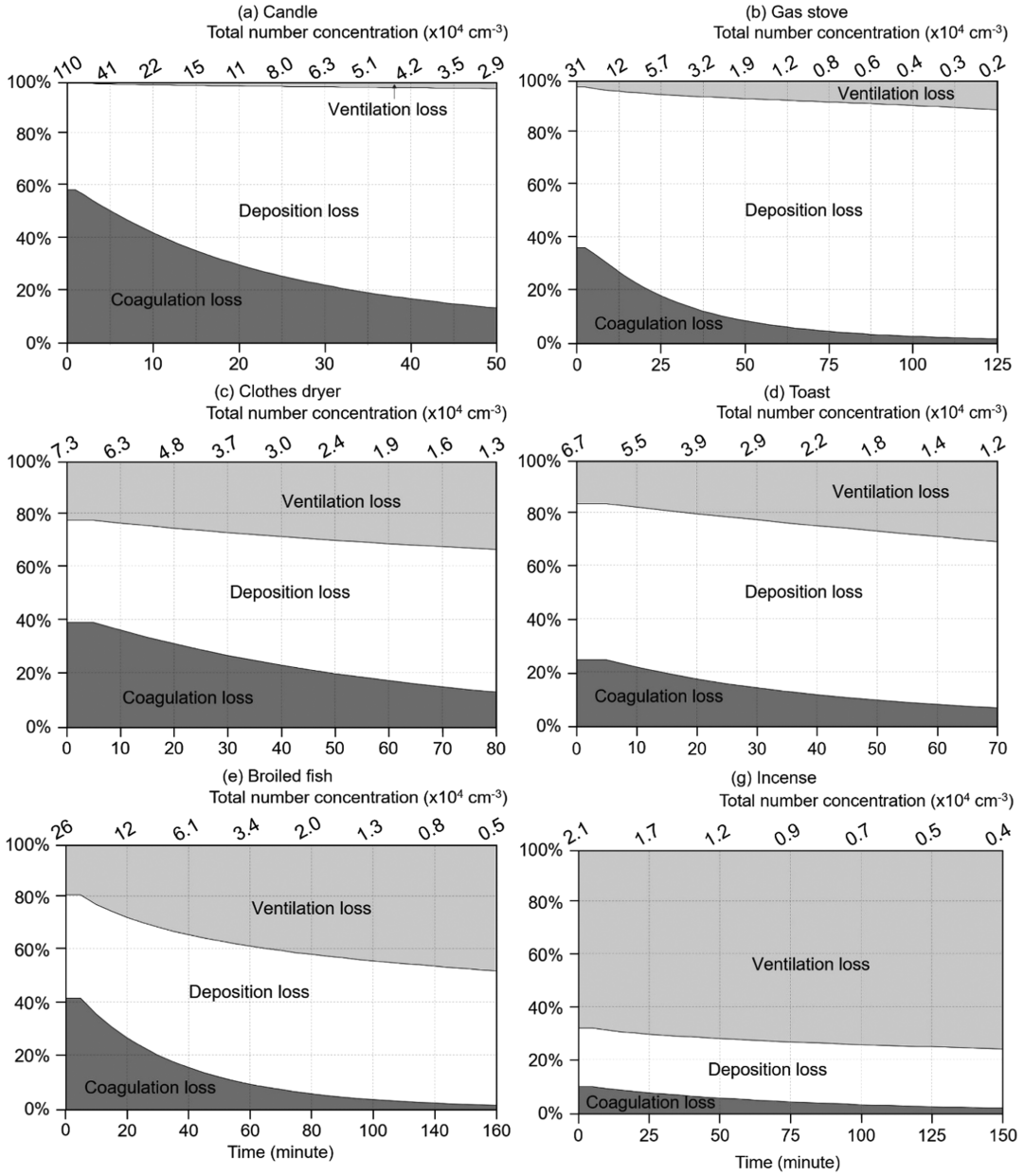

Figure 6. Relative contributions of coagulation, deposition, and ventilation to particle number concentration loss with time over the decay period for the six indoor sources: (a) candle, (b) gas stove, (c) clothes dryer, (d) toast, (e) broiled fish, and (f) incense. Note the different scales of total number concentration for six indoor sources.

particle concentrations. For the sources that yield high number concentrations of sub-10 nm particles such as candle and gas stove (Figure 6a,b), coagulation and deposition are primarily responsible for the particle number loss. For example, regarding the candle burning, the total particle number concentration was 1.1×10^6 cm^{-3} at the beginning of decay and coagulation and deposition account for up to 59 and 40% of the total particle number loss, respectively. However, after 50 min of the decay, coagulation was responsible for only 15% of the total particle number loss, while deposition was responsible for 80% of the total loss. Note that ventilation loss accounted for less than 0.3% of the total particle number loss over the whole decay. The results with the gas stove showed a total particle number concentration of 3.1×10^5 cm^{-3} at the beginning of decay and the initial contributions of coagulation, deposition, and ventilation to the total particle number loss were 37, 61, and 2.2%, respectively. In this case, the effect of deposition was higher than coagulation mainly due to relatively larger particle sizes with smaller concentrations compared to the candle data. For the clothes dryer and indoor cooking activities (toast and broiled fish), coagulation and deposition still accounted for more than 50% of the total particle number loss over the decay. However, ventilation losses were considerably high compared to those of the candle and gas stove, which was mainly attributed to higher air change rates (clothes dryer 0.36 h^{-1}, toast 0.34 h^{-1}, broiled fish 0.59 h^{-1}) and larger particle sizes that reduced the effect of coagulation. In the case of incense, the ventilation effect was highest (up to 75%) among the six emission sources because of the low total particle number concentration (<2.1×10^4 cm^{-3}) with the majority of particles in the size range of >100 nm.

https://doi.org/10.1021/acs.est.0c08739
Environ. Sci. Technol. XXXX, XXX, XXX−XXX

The present study reveals that all three aerosol loss mechanisms, i.e., coagulation, deposition, and ventilation, can meaningfully influence indoor particle size and concentration dynamics depending on the emission source type and indoor environmental condition.[37,53,54] Given that this study has examined the particle dynamics in residential buildings based on the transient, well-mixed material balance model, future studies are warranted to examine how the spatial inhomogeneity of particle concentrations affects the measurement and model uncertainties under representative incomplete air mixing conditions.[55]

■ ASSOCIATED CONTENT

Supporting Information

The Supporting Information is available free of charge at https://pubs.acs.org/doi/10.1021/acs.est.0c08739.

(1) Description of measurements; (2) description of the six episodic sources; (3) monitoring of size-resolved particles; (4) particle size distributions (dN/d(logDp)); (5) particle number concentrations; (6) modeling of coagulation; (7) model prediction errors; (8) time variations of first-order equivalent coagulation loss rates; (9) size-resolved deposition rates for individual emission sources; and (10) size-resolved particle number concentration over time: measurement vs model (PDF)

■ AUTHOR INFORMATION

Corresponding Author

Donghyun Rim − *Department of Architectural Engineering, Pennsylvania State University, University Park, Pennsylvania 16802, United States;* orcid.org/0000-0002-0751-3605; Email: drim@psu.edu

Authors

Su-Gwang Jeong − *Department of Architectural Engineering, Soongsil University, Seoul 06978, Republic of Korea*

Lance Wallace − *Wallace Research, Santa Rosa, California 95409, United States;* orcid.org/0000-0002-6635-2303

Complete contact information is available at: https://pubs.acs.org/10.1021/acs.est.0c08739

Notes

The authors declare no competing financial interest.

■ ACKNOWLEDGMENTS

The research presented in this paper was supported by the U.S. National Science Foundation (NSF Grant 1944325) and the Basic Science Research Program through the National Research Foundation of Korea funded by the Ministry of Education (NRF-2020R1A6A1A03044977).

■ REFERENCES

(1) Morawska, L.; Ayoko, G.; Bae, G.; Buonanno, G.; Chao, C.; Clifford, S.; Fu, S. C.; Hänninen, O.; He, C.; Isaxon, C.; et al. Airborne particles in indoor environment of homes, schools, offices and aged care facilities: The main routes of exposure. *Environ. Int.* **2017**, *108*, 75−83.

(2) Brook, R. D.; Rajagopalan, S.; Pope, C. A., III; Brook, J. R.; Bhatnagar, A.; Diez-Roux, A. V.; Holguin, F.; Hong, Y.; Luepker, R. V.; Mittleman, M. A.; et al. Particulate matter air pollution and cardiovascular disease: an update to the scientific statement from the American Heart Association. *Circulation* **2010**, *121*, 2331−2378.

(3) Janssen, N. A.; Hoek, G.; Simic-Lawson, M.; Fischer, P.; Van Bree, L.; Ten Brink, H.; Keuken, M.; Atkinson, R. W.; Anderson, H. R.; Brunekreef, B.; et al. Black carbon as an additional indicator of the adverse health effects of airborne particles compared with PM10 and PM2. 5. *Environ. Health Perspect.* **2011**, *119*, 1691−1699.

(4) Deng, Q.; Lu, C.; Yu, Y.; Li, Y.; Sundell, J.; Norbäck, D. Early life exposure to traffic-related air pollution and allergic rhinitis in preschool children. *Respir. Med.* **2016**, *121*, 67−73.

(5) Norbäck, D.; Lu, C.; Zhang, Y.; Li, B.; Zhao, Z.; Huang, C.; Zhang, X.; Qian, H.; Sundell, J.; Deng, Q. Common cold among preschool children in China-associations with ambient PM10 and dampness, mould, cats, dogs, rats and cockroaches in the home environment. *Environ. Int.* **2017**, *103*, 13−22.

(6) Organization, W. H. *Health Effects of Black Carbon*; WHO, 2012.

(7) De Kluizenaar, Y.; Kuijpers, E.; Eekhout, I.; Voogt, M.; Vermeulen, R.; Hoek, G.; Sterkenburg, R.; Pierik, F.; Duyzer, J.; Meijer, E.; et al. Personal exposure to UFP in different microenvironments and time of day. *Build. Environ.* **2017**, *122*, 237−246.

(8) Ruan, T.; Rim, D. Indoor air pollution in office buildings in mega-cities: Effects of filtration efficiency and outdoor air ventilation rates. *Sustainable Cities Soc.* **2019**, *49*, No. 101609.

(9) Riley, W. J.; McKone, T. E.; Lai, A. C.; Nazaroff, W. W. Indoor particulate matter of outdoor origin: importance of size-dependent removal mechanisms. *Environ. Sci. Technol.* **2002**, *36*, 200−207.

(10) Wallace, L. A decade of studies of human exposure: what have we learned? *Risk Anal.* **1993**, *13*, 135−139.

(11) Klepeis, N. E.; Nelson, W. C.; Ott, W. R.; Robinson, J. P.; Tsang, A. M.; Switzer, P.; Behar, J. V.; Hern, S. C.; Engelmann, W. H. The National Human Activity Pattern Survey (NHAPS): a resource for assessing exposure to environmental pollutants. *J. Exposure Sci. Environ. Epidemiol.* **2001**, *11*, 231−252.

(12) Awada, M.; Becerik-Gerber, B.; Hoque, S.; O'Neill, Z.; Pedrielli, G.; Wen, J.; Wu, T. Ten questions concerning occupant health in buildings during normal operations and extreme events including the COVID-19 pandemic. *Build. Environ.* **2021**, *188*, No. 107480.

(13) Long, C. M.; Suh, H. H.; Koutrakis, P. Characterization of indoor particle sources using continuous mass and size monitors. *J. Air Waste Manage. Assoc.* **2000**, *50*, 1236−1250.

(14) Rim, D.; Choi, J.-I.; Wallace, L. A. Size-resolved source emission rates of indoor ultrafine particles considering coagulation. *Environ. Sci. Technol.* **2016**, *50*, 10031−10038.

(15) Nel, A.; Xia, T.; Mädler, L.; Li, N. Toxic potential of materials at the nanolevel. *Science* **2006**, *311*, 622−627.

(16) Kim, S.; Choi, J. E.; Choi, J.; Chung, K.-H.; Park, K.; Yi, J.; Ryu, D.-Y. Oxidative stress-dependent toxicity of silver nanoparticles in human hepatoma cells. *Toxicol. In Vitro* **2009**, *23*, 1076−1084.

(17) Cho, M.; Cho, W.-S.; Choi, M.; Kim, S. J.; Han, B. S.; Kim, S. H.; Kim, H. O.; Sheen, Y. Y.; Jeong, J. The impact of size on tissue distribution and elimination by single intravenous injection of silica nanoparticles. *Toxicol. Lett.* **2009**, *189*, 177−183.

(18) Corsi, R. L.; Siegel, J. A.; Chiang, C. Particle resuspension during the use of vacuum cleaners on residential carpet. *J. Occup. Environ. Hyg.* **2008**, *5*, 232−238.

(19) Pagels, J.; Wierzbicka, A.; Nilsson, E.; Isaxon, C.; Dahl, A.; Gudmundsson, A.; Swietlicki, E.; Bohgard, M. Chemical composition and mass emission factors of candle smoke particles. *J. Aerosol Sci.* **2009**, *40*, 193−208.

(20) Slezakova, K.; Pereira, M.; Alvim-Ferraz, M. Influence of tobacco smoke on the elemental composition of indoor particles of different sizes. *Atmos. Environ.* **2009**, *43*, 486−493.

(21) Glytsos, T.; Ondráček, J.; Džumbová, L.; Kopanakis, I.; Lazaridis, M. Characterization of particulate matter concentrations during controlled indoor activities. *Atmos. Environ.* **2010**, *44*, 1539−1549.

(22) Abdullahi, K. L.; Delgado-Saborit, J. M.; Harrison, R. M. Emissions and indoor concentrations of particulate matter and its specific chemical components from cooking: A review. *Atmos. Environ.* **2013**, *71*, 260−294.

(23) Wallace, L.; Wang, F.; Howard-Reed, C.; Persily, A. Contribution of gas and electric stoves to residential ultrafine particle concentrations between 2 and 64 nm: size distributions and emission and coagulation rates. *Environ. Sci. Technol.* **2008**, *42*, 8641−8647.
(24) Salthammer, T.; Schripp, T.; Uhde, E.; Wensing, M. Aerosols generated by hardcopy devices and other electrical appliances. *Environ. Poll* **2012**, *169*, 167−174.
(25) Wallace, L.; Howard-Reed, C. Continuous monitoring of ultrafine, fine, and coarse particles in a residence for 18 months in 1999-2000. *J. Air Waste Manage. Assoc.* **2002**, *52*, 828−844.
(26) Wallace, L. A.; Emmerich, S. J.; Howard-Reed, C. Source strengths of ultrafine and fine particles due to cooking with a gas stove. *Environ. Sci. Technol.* **2004**, *38*, 2304−2311.
(27) Wallace, L.; Ott, W. Personal exposure to ultrafine particles. *J. Exposure Sci. Environ. Epidemiol.* **2011**, *21*, 20−30.
(28) Ferro, A. R.; Kopperud, R. J.; Hildemann, L. M. Source strengths for indoor human activities that resuspend particulate matter. *Environ. Sci. Technol.* **2004**, *38*, 1759−1764.
(29) Gomes, C.; Freihaut, J.; Bahnfleth, W. Resuspension of allergen-containing particles under mechanical and aerodynamic disturbances from human walking. *Atmos. Environ.* **2007**, *41*, 5257−5270.
(30) Hinds, W., *Aerosol Technology*, Wiley, New York, 1982.
(31) Friedlander, S.; Smoke, D.; Haze, J. W. Sons. New York 1977.
(32) Willeke, K.; Baron, P. A.; Martonen, T. *Aerosol Measurement: Principles, Techniques, and Applications*; Van Nostrand Reinhold: New York, 1993; Vol. *876*.
(33) Rim, D.; Green, M.; Wallace, L.; Persily, A.; Choi, J.-I. Evolution of ultrafine particle size distributions following indoor episodic releases: relative importance of coagulation, deposition and ventilation. *Aerosol Sci. Technol.* **2012**, *46*, 494−503.
(34) Wallace, L. Indoor sources of ultrafine and accumulation mode particles: size distributions, size-resolved concentrations, and source strengths. *Aerosol Sci. Technol.* **2006**, *40*, 348−360.
(35) Wallace, L. Indoor particles: a review. *J. Air Waste Manage. Assoc.* **1996**, *46*, 98−126.
(36) Wallace, L.; Jeong, S. G.; Rim, D. Dynamic behavior of indoor ultrafine particles (2.3-64 nm) due to burning candles in a residence. *Indoor Air* **2019**, *29*, 1018−1027.
(37) Lai, A. C.; Chen, J. Numerical study of cooking particle coagulation by using an Eulerian model. *Build. Environ.* **2015**, *89*, 38−47.
(38) Géhin, E.; Ramalho, O.; Kirchner, S. Size distribution and emission rate measurement of fine and ultrafine particle from indoor human activities. *Atmos. Environ.* **2008**, *42*, 8341−8352.
(39) Stabile, L.; De Luca, G.; Pacitto, A.; Morawska, L.; Avino, P.; Buonanno, G. Ultrafine particle emission from floor cleaning products. *Indoor Air* **2021**, *31*, 63−73.
(40) Wang, Y.; Chen, L.; Chen, R.; Tian, G.; Li, D.; Chen, C.; Ge, X.; Ge, G. Effect of relative humidity on the deposition and coagulation of aerosolized SiO2 nanoparticles. *Atmos. Res.* **2017**, *194*, 100−108.
(41) Ogulei, D.; Hopke, P.; Wallace, L. Analysis of indoor particle size distributions in an occupied townhouse using positive matrix factorization. *Indoor Air* **2006**, *16*, 204−215.
(42) Jacobson, M. Z.; Jacobson, M. Z. *Fundamentals of Atmospheric Modeling*; Cambridge University Press, 2005.
(43) Hussein, T.; Korhonen, H.; Herrmann, E.; Hämeri, K.; Lehtinen, K. E.; Kulmala, M. Emission rates due to indoor activities: indoor aerosol model development, evaluation, and applications. *Aerosol Sci. Technol.* **2005**, *39*, 1111−1127.
(44) Anand, S.; Mayya, Y. Modeling Critical Air Exchange Rates (CAERs) for aerosol number concentrations from nano-particle sources using an "effective coagulation coefficient" approach. *Aerosol Sci. Technol.* **2017**, *51*, 421−429.
(45) Anand, S.; Sreekanth, B.; Mayya, Y. S. Effective coagulation coefficient approach for estimating particle number emission rates for strong emission sources. *Aerosol Air Qual. Res.* **2016**, *16*, 1541−1547.
(46) Lai, A. C. K.; Nazaroff, W. W. Modeling indoor particle deposition from turbulent flow onto smooth surfaces. *J. Aerosol Sci.* **2000**, *31*, 463−476.
(47) Nazaroff, W. W. Indoor particle dynamics. *Indoor Air* **2004**, *14*, 175−183.
(48) Thatcher, T. L.; Lai, A. C.; Moreno-Jackson, R.; Sextro, R. G.; Nazaroff, W. W. Effects of room furnishings and air speed on particle deposition rates indoors. *Atmos. Environ.* **2002**, *36*, 1811−1819.
(49) Pnueli, D.; Gutfinger, C.; Fichman, M. A turbulent-Brownian model for aerosol coagulation. *Aerosol Sci. Technol.* **1991**, *14*, 201−209.
(50) Lin, J.; Pan, X.; Yin, Z.; Ku, X. Solution of general dynamic equation for nanoparticles in turbulent flow considering fluctuating coagulation. *Appl. Math. Mech.* **2016**, *37*, 1275−1288.
(51) Hussein, T.; Hruška, A.; Dohányosová, P.; Džumbová, L.; Hemerka, J.; Kulmala, M.; Smolík, J. Deposition rates on smooth surfaces and coagulation of aerosol particles inside a test chamber. *Atmos. Environ.* **2009**, *43*, 905−914.
(52) Wallace, L. A.; Emmerich, S. J.; Howard-Reed, C. Effect of central fans and in-duct filters on deposition rates of ultrafine and fine particles in an occupied townhouse. *Atmos. Environ.* **2004**, *38*, 405−413.
(53) Zhao, Y.; Wang, F.; Zhao, J. Size-resolved ultrafine particle deposition and Brownian coagulation from gasoline vehicle exhaust in an environmental test chamber. *Environ. Sci. Technol.* **2015**, *49*, 12153−12160.
(54) Schnell, M.; Cheung, C.; Leung, C. Investigation on the coagulation and deposition of combustion particles in an enclosed chamber with and without stirring. *J. Aerosol Sci.* **2006**, *37*, 1581−1595.
(55) Ahn, H.; Rim, D.; Lo, L. J. Ventilation and energy performance of partitioned indoor spaces under mixing and displacement ventilation. *Build. Simul.* **2018**, *11*, 561−574.

https://doi.org/10.1021/acs.est.0c08739
Environ. Sci. Technol. XXXX, XXX, XXX−XXX